Emergence of oblique dunes in a landscape-scale experiment

Lü Ping[1,2], Clément Narteau[2], Zhibao Dong[1],
Zhengcai Zhang[1], Sylvain Courrech du Pont[3]

[1] Key Laboratory of Desert and Desertification, Cold and Arid Regions Environmental and Engineering Research Institute, Chinese Academy of Sciences, 320 West Donggang Road, 730000 Lanzhou, Gansu, China.

[2] Institut de Physique du Globe de Paris, Sorbonne Paris Cité, Univ Paris Diderot, UMR 7154 CNRS, 1 rue Jussieu, 75238 Paris, Cedex 05, France.

[3] Laboratoire Matière et Système Complexes, Sorbonne Paris Cité, Univ Paris Diderot, UMR 7057 CNRS, Bâtiment Condorcet, 10 rue Alice Domon et Léonie Duquet, 75205 Paris Cedex 13, France.

Contents

Figure 1: Grain size distribution in the Tengger desert. The sand bed exhibits a mean grain size of 2.39 (d=190 μm).

The landscape-scale experiment site is located close to the oasis city of Shapotu at 8 km from the Yellow River in the Tengger desert, which covers an area of about 36,700 km^2 in the northwest part of the Zhongwei County in the Ningxia Hui Autonomous Region of the People's Republic of China (37° 31´ N, 105° E). This desert is characterised by a lognormal grain size distribution with a mean value d=190 μm (Fig. 1).

1 Characterisation of the wind regime and sediment transport from in-situ continuous measurements

An automatic wind measurement system was installed in the centre of the flattened area just south of the three experimental plots. This system contains a wind speed sensor, a wind direction sensor and a data logger. The EC9-1 wind sensors that integrate both wind speed and direction measurements has been developed by the Changchun Meteorological Instrument Research Institute. To store the wind data, a CR200 data loggers developed by the Campbell Scenic, Inc. have been used. These data loggers were wrapped in carpets and buried 0.5 m under the ground to ensure a proper functioning of this material at high and low external temperatures. Wind sensors are located at the top of a meteorological tower at a height of 10 m

(see Fig. 4 and Figs. 1a,b of the main manuscript). The wind measurement system records the mean wind speed and direction every minute. The discussion below is based on four consecutive years of complete data from the 1$^{\text{th}}$ of January 2008 to the 31$^{\text{th}}$ of December 2011 (Fig. 1c of the main manuscript).

Raw wind data shows lot of variability in direction and strength reflecting the turbulent character of the air flow at the Earth's surface. Nevertheless, there is a dominant bimodal wind regime resulting from the global climatic forcing in this region. In what follows, we propose a general method to estimate the direction and the relative strength of the prevailing winds from the data. Before we need to recall how we estimate sediment transport from the wind data. Then, we will be able to discuss not only the wind patterns but also the magnitude and the direction of the sediment fluxes that directly contribute to dune morphodynamics.

1.1 Estimation of sediment transport from wind data

Wind measurements provide the wind speed u^i and the wind direction $\mathbf{x}_i$ at different times t_i, $i \in [1, N]$. Considering that these wind properties have been measured at a given height z, the shear velocity can be defined as

$$u_*^i = \frac{u_i \kappa}{\log(z/z_0)} \tag{1}$$

where $z_0 = 10^{-3}$ m is the surface roughness length and $\kappa = 0.4$ is the von-Kármán constant.

The threshold shear velocity value for motion inception can be determined using the formula calibrated by *Iversen and Rasmussen* [1999],

$$u_{\text{c}} = 0.1 \sqrt{\frac{\rho_s}{\rho_f} g d}, \tag{2}$$

where g is the gravitational acceleration, ρ_s/ρ_f is the grain to fluid density ratio and d is the grain diameter. Then, the saturated sand flux on a flat erodible bed can be determined using a relationship proposed by *Ungar and Haff* [1987],

$$Q_{\text{sat}}(u_*) = \begin{cases} 22 \frac{\rho_f}{\rho_s} \sqrt{\frac{d}{g}} \left(u_*^2 - u_c^2 \right) & \text{for } u_* \geq u_{\text{c}}, \\ 0 & \text{else.} \end{cases} \tag{3}$$

In practise, for a given time period around t_i, the sand flux vector over a flat sand bed can be written

$$\mathbf{Q}_{\text{sat}}^i = Q_{\text{sat}}(u_*^i)\mathbf{x}_i. \tag{4}$$

Thus, it is possible to estimate the total sand flux, also called the drift potential,

$$Q = \text{DP} = \frac{\sum_{i=2}^{N} \|\mathbf{Q}_{\text{sat}}^i\|(t_i - t_{i-1})}{\sum_{i=2}^{N}(t_i - t_{i-1})}, \tag{5}$$

as well as the resultant drift potential

$$\text{RDP} = \frac{\left\| \sum_{i=2}^{N}(t_i - t_{i-1})\mathbf{Q}_{\text{sat}}^i \right\|}{\sum_{i=2}^{N}(t_i - t_{i-1})}, \tag{6}$$

and the resultant drift direction, RDD, which is the angle of the RDP measured anticlockwise from East.

1.2   Wind and sand flux patterns

Fig. 1c of the main manuscript shows the wind and sand flux roses in Shapotu for a time period of four years from the 1th of January 2008 to the 31th of December 2011. These roses gives the angular dispersion of air flow and sediment transport, respectively. There is a clear bimodal wind regime with a primary peak in the southeast direction and a secondary peak in the west direction. As shown by Fig. 2, these different wind orientations may be associated to seasonal variations.

During winter, heat loss in the ultra-continental region of Central Asia leads to the development of a persistent, large and intense thermal anticyclone centred over Mongolia and eastern Siberia. Calm, dry air dominates most of the desert areas, with clockwise circulation radiating from the central area of high pressure. This circulating flow moves northwest winds across western China. In summer the surface of the Asian continent gains heat and the dominant atmospheric systems are thermal depressions. This counterclockwise circulation results in easterly and southerly winds in this southern part of the Gobi desert.

The strongest winds are observed during the spring when the difference of temperature between central and eastern Asia is the highest. In addition, to these seasonal variations, there are also strong variations of wind strength during the day (Fig. 3) with a clear maximum around 2 pm. During the night, the dominant wind is always from the the northwest whatever the season.
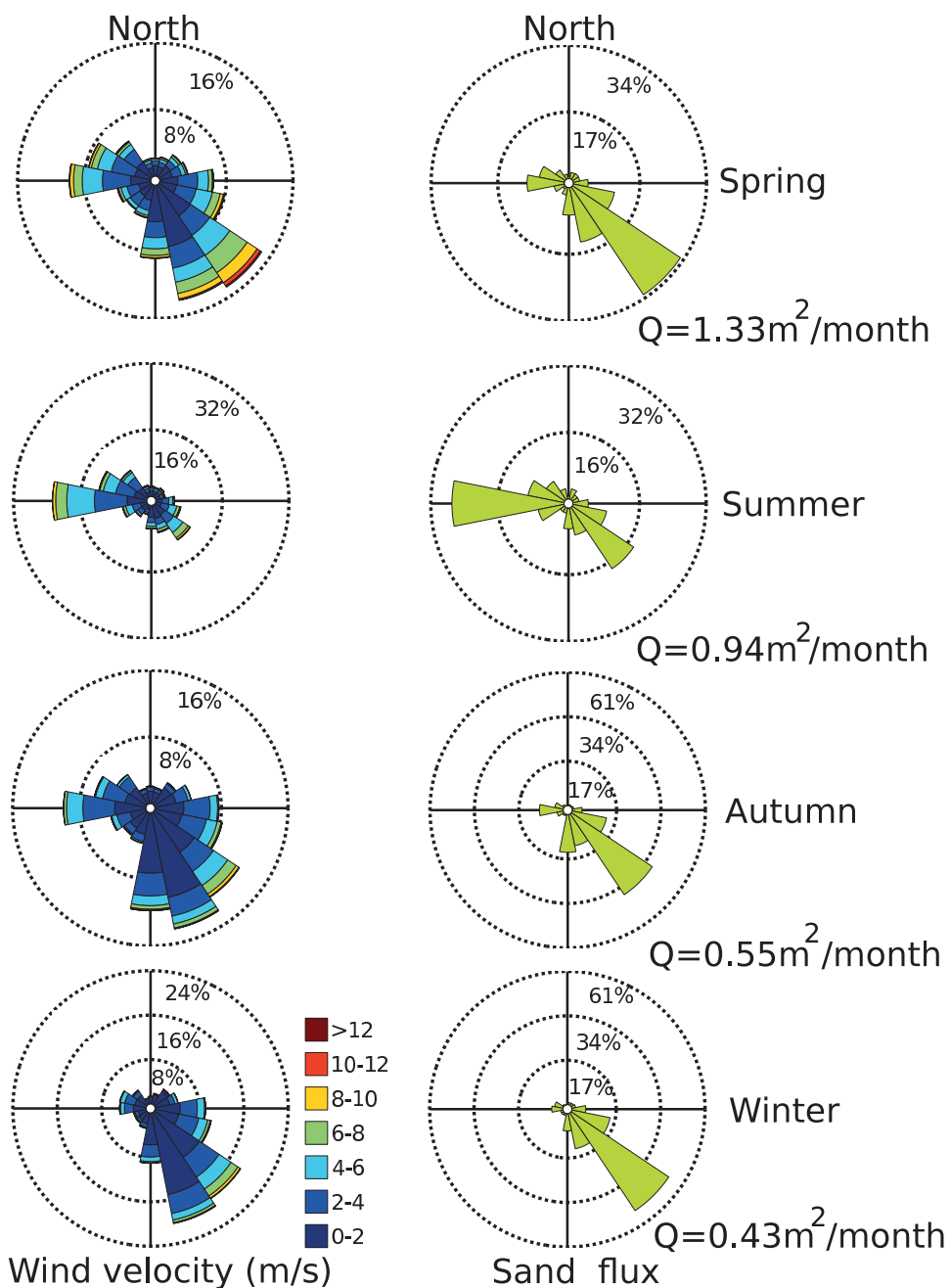
Figure 2: The seasonal wind regimes in Shapotu from the 1th of January 2008 to the 31th of December 2011. In winter, cold, calm and dry air in Siberia are responsible for northwesterly winds in the Tengger desert. In Summer, thermal depressions induced by the East Asian monsoon produce easterly winds. From the sediment fluxes, we can observe that, in addition to changes in orientation, there are also seasonal variations of wind strength.
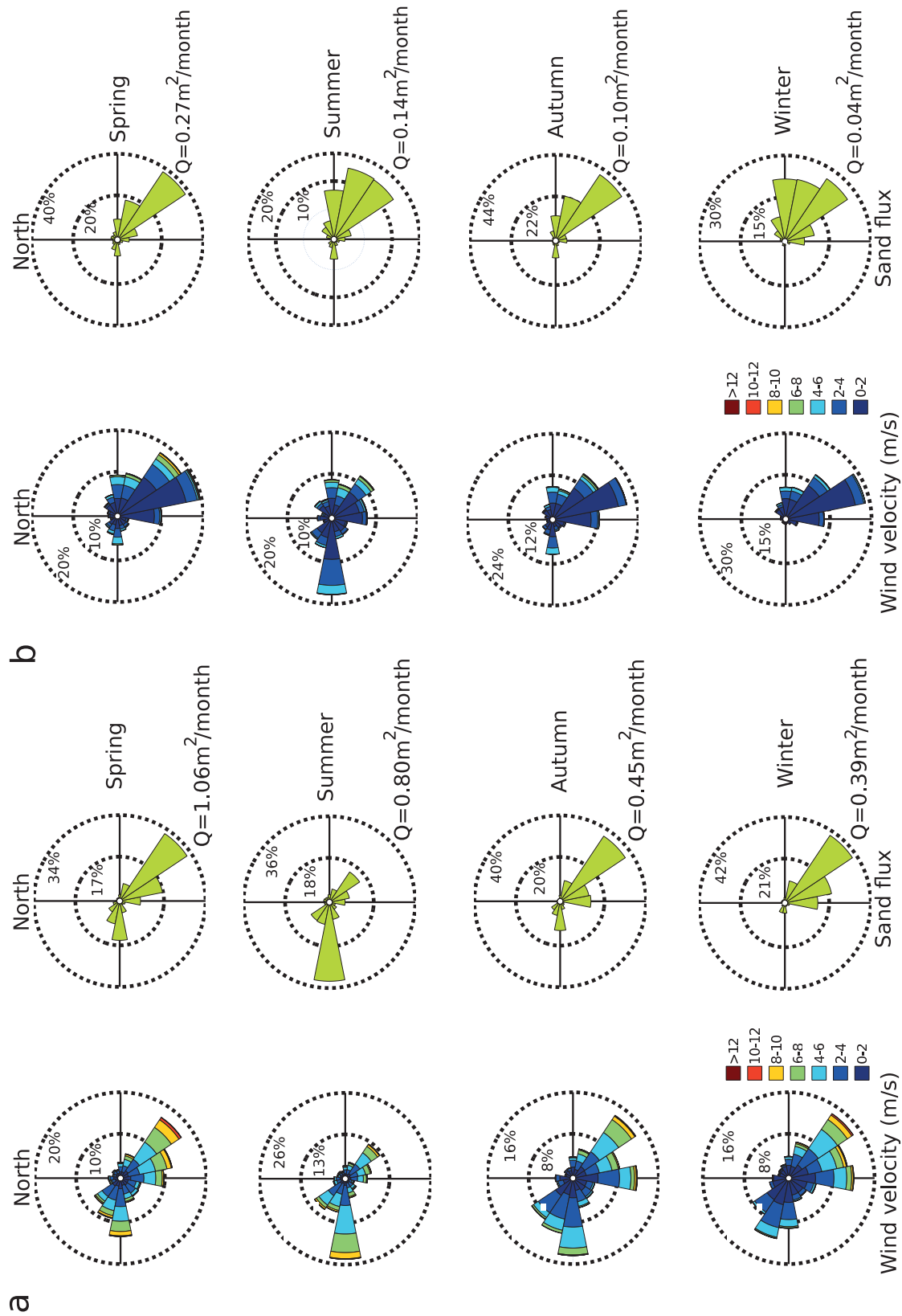
Figure 3: Seasonal wind and sand flux patterns in the experimental plot according to day and night from the 1th of January 2008 to the 31st of December 2011. Diurnal and nocturnal wind and sand flux roses (a) from 7 am to 7 pm and (b) from 7 pm to 7 am, respectively. Strongest wind are recorded during the day. At night, there is no significant seasonal variation of sand flux orientation.

2 Topographic surveys in the landscape-scale experiment

Starting from a flat sand bed on the 20th of December 2007, the dunefield topography of the open corridor and the closed area have been measured on the

[1] 30th of April 2008 (Fig. 6a).

[2] 31st of March 2009 (Fig. 7a).

[3] 31st of October 2009 (Fig. 8a).

[4] 1st of June 2010 (Fig. 9a).

[5] 31st of October 2010 (Fig. 10a).

[6] 30th of April 2011 (Fig. 11a).

[7] 31st of October 2011 (Fig. 12a).

Fig. 4 shows the landscape scale experiment site and the three experimental plots on the 26th of August 2011. On the same date, Fig. 5 shows the emergent oblique dune features after almost four years of the ongoing experiment.

3 Quantitative characterisation of bedform orientation using the mass distribution

In this section, we present a general method to provide quantitative and reproducible characterisation of all types of topographic measurements. When applied to dunefields we will show that this method can be used to infer the principal bedform orientation but also their variability.

At a given time t, let us consider a dunefield topography $h(x, y)$, renamed h in what follows for sake of readability. An isolated dune is defined as a topographic anomaly above a given threshold elevation h_t. According to this elevation, each dune d is associated with an isoline $\mathcal{C}_\mathrm{d}$ surrounding a flat and horizontal closed surface $\mathcal{S}_d$. The volume of the dune is given by

$$\mathcal{V}_\mathrm{d} = \iint_{\mathcal{S}_\mathrm{d}} (h - h_\mathrm{t}) \, \mathrm{d}x \, \mathrm{d}y. \tag{7}$$

Using the same topography, we characterise each dune by the two first moments of the distribution of mass. The first moment gives the position of
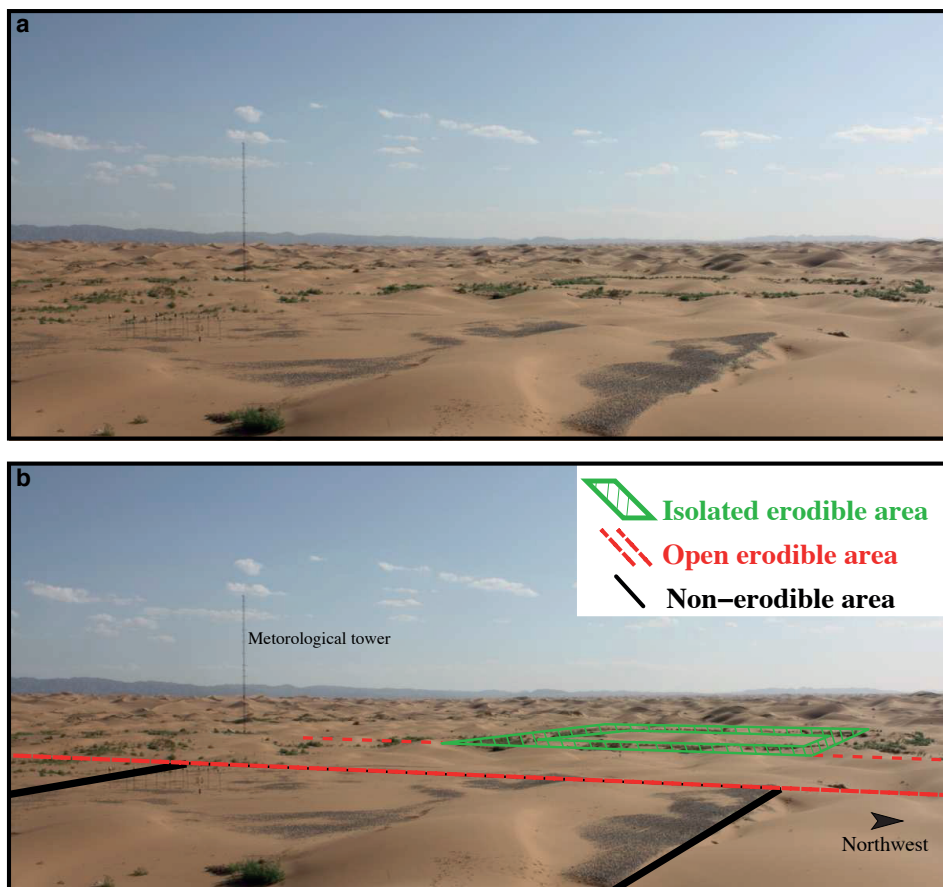
Figure 4: The three experimental plots on the 26th of August 2011. (a) Picture of the landscape scale experiment site taken from the northern corner of the non-erodible bed (see Figs. 1a,b of the main manuscript). (b) Same picture with legends. The red lines are the limits of the open corridor with an erodible bed. The black square shows the open area with the non-erodible bed covered with gravels. Between the two green squares a straw checkerboard isolates an erodible bed from external sand fluxes. For scale, remember that the meteorological tower has a height of 10 m and that both the closed area and the non-erodible bed are squares of 80×80 m^2. Abundant precipitations during summer 2011 explain the relatively high vegetation cover. Note how this vegetation grow more easily over the straw checkerboard protecting the closed area from external sand fluxes (dashed green area in b) due to smaller bed shear stress (see Methods in the main manuscript).

East

Southeast
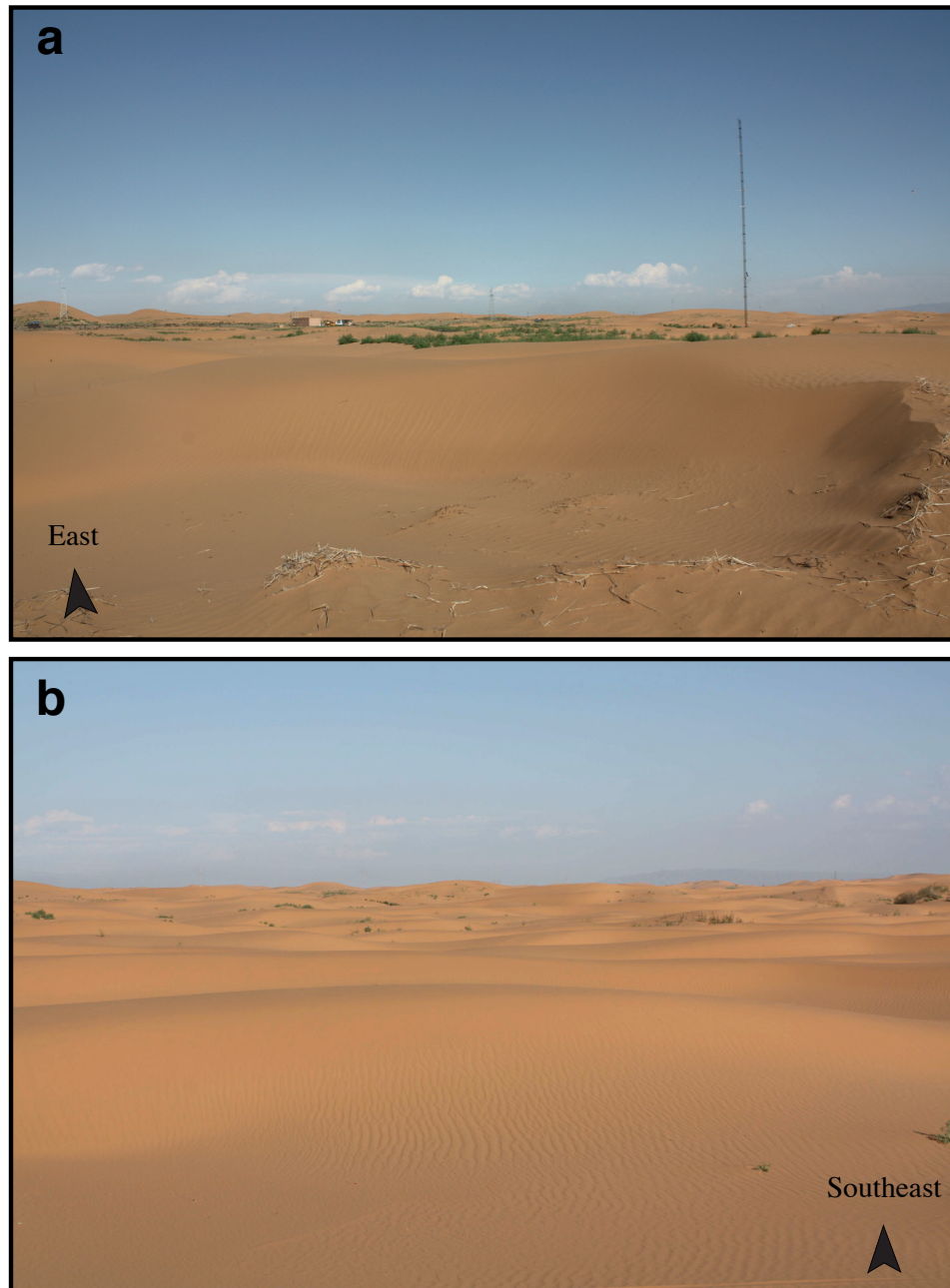
Figure 5: Dunes in the landscape scale experiment site on the 26ᵗʰ of August 2011. (a) Picture of the three experimental plots taken from the western corner of the closed area (see Figs. 1a,b of the main manuscript). We recognise the inner corner of the straw checkerboard in the bottom right and the house close to the road on the other side. (b) Picture of the dunes developing in the flattened area outside the three experimental plots at 50 m south of the meteorological tower (see Figs. 1a,b of the main manuscript). Note the characteristic wavelength of the bedforms as well as the step in dune size at the boundary of the flattened area.

the centre of mass. The second moment estimates the dispersion of mass in 3D. It is the covariance matrix or the so-called mass distribution matrix.

3.1 The centre of mass

The coordinates of the centre of mass μ are given by

$$\mu_x = \iint_{\mathcal{S}_d} \int_{h_\mathrm{t}}^{h} x \, \mathrm{d}x \, \mathrm{d}y \, \mathrm{d}z \ = \iint_{\mathcal{S}_d} x \cdot h \, \mathrm{d}x \, \mathrm{d}y \tag{8}$$

$$\mu_y = \iint_{\mathcal{S}_d} \int_{h_\mathrm{t}}^{h} y \, \mathrm{d}x \, \mathrm{d}y \, \mathrm{d}z \ = \iint_{\mathcal{S}_d} y \cdot h \, \mathrm{d}x \, \mathrm{d}y \tag{9}$$

$$\mu_z = \iint_{\mathcal{S}_d} \int_{h_\mathrm{t}}^{h} z \, \mathrm{d}x \, \mathrm{d}y \, \mathrm{d}z \ = \iint_{\mathcal{S}_d} \frac{h^2}{2} \, \mathrm{d}x \, \mathrm{d}y \tag{10}$$

In Figs. 3d,4c of the main manuscript, dune migration vectors correspond to the displacement of the centre of mass of individual dune features during specific time intervals.

3.2 The mass distribution matrix

The second moment of the distribution of mass is a 3×3 matrix $\mathcal{M}$. Each element $\mathcal{M}_{ij}$ of this matrix is defined as

$$\mathcal{M}_{ij} = \widetilde{\mathcal{M}}_{ij} - \mu_i \mu_j. \tag{11}$$

where

$$\widetilde{\mathcal{M}}_{xx} = \iint_{\mathcal{S}_d} \int_{h_\mathrm{t}}^{h} x^2 \, \mathrm{d}x \, \mathrm{d}y \, \mathrm{d}z \ = \iint_{\mathcal{S}_d} x^2 \cdot h \, \mathrm{d}x \, \mathrm{d}y \tag{12}$$

$$\widetilde{\mathcal{M}}_{yy} = \iint_{\mathcal{S}_d} \int_{h_\mathrm{t}}^{h} y^2 \, \mathrm{d}x \, \mathrm{d}y \, \mathrm{d}z \ = \iint_{\mathcal{S}_d} y^2 \cdot h \, \mathrm{d}x \, \mathrm{d}y \tag{13}$$

$$\widetilde{\mathcal{M}}_{zz} = \iint_{\mathcal{S}_d} \int_{h_\mathrm{t}}^{h} z^2 \, \mathrm{d}x \, \mathrm{d}y \, \mathrm{d}z \ = \iint_{\mathcal{S}_d} \frac{h^3}{3} \, \mathrm{d}x \, \mathrm{d}y \tag{14}$$

$$\widetilde{\mathcal{M}}_{xy} = \iint_{\mathcal{S}_d} \int_{h_\mathrm{t}}^{h} x \cdot y \, \mathrm{d}x \, \mathrm{d}y \, \mathrm{d}z \ = \iint_{\mathcal{S}_d} x \cdot y \cdot h \, \mathrm{d}x \, \mathrm{d}y \tag{15}$$

$$\widetilde{\mathcal{M}}_{xz} = \iint_{\mathcal{S}_d} \int_{h_\mathrm{t}}^{h} x \cdot z \, \mathrm{d}x \, \mathrm{d}y \, \mathrm{d}z \ = \iint_{\mathcal{S}_d} \frac{x \cdot h^2}{2} \, \mathrm{d}x \, \mathrm{d}y \tag{16}$$

$$\widetilde{\mathcal{M}}_{yz} = \iint_{\mathcal{S}_d} \int_{h_\mathrm{t}}^{h} y \cdot z \, \mathrm{d}x \, \mathrm{d}y \, \mathrm{d}z \ = \iint_{\mathcal{S}_d} \frac{y \cdot h^2}{2} \, \mathrm{d}x \, \mathrm{d}y \tag{17}$$

We calculate the eigenvectors $\mathbf{V}_{1,2,3}$ and the corresponding eigenvalues $\lambda_1 \geq \lambda_2 \geq \lambda_3$ of the square matrix $\mathcal{M}$ to characterise the principal orientations of the topographic anomaly. Obviously, these eigenstates may characterise quantitatively the major morphological dune types. Nevertheless, it

depends on the threshold elevation h_{t}, which should be chosen according to the characteristic wavelength and the amplitude of the dune patterns.

For the analysis of linear dunes (e. g. Figs. 6-12a), the following properties are of special interest :

- The primary orientation $\mathbf{V}_1$ corresponds to the largest eigenvalue λ_1 and gives, in a vast majority of cases, the direction of the crest (Figs. 6-12b,c).

- The secondary orientation $\mathbf{V}_2$ is also horizontal because the height of dunes is always small when compare to their horizontal dimensions. Then, in a vast majority of cases, $\mathbf{V}_2$ is perpendicular to the crest.

- As the repose angle is approximately 35°, the tertiary orientation $\mathbf{V}_3$ is vertical.

It is important to note that the eigenvalue may give the dune aspect ratio in different directions. In addition, the evolution of the diagonal and non-diagonal components of the mass distribution matrix can also be used to estimate stretching and shearing deformation of dune shape.

3.3 Identification of crests and valleys using a digital elevation map

In order to locate crests and valleys within a dunefield, we first calculate the gradient of the digital elevation map $h(x, y)$

$$\boldsymbol{\nabla} h = \frac{\partial h}{\partial x}\,\mathbf{e_x} + \frac{\partial h}{\partial y}\,\mathbf{e_y} \tag{18}$$

and its norm

$$\|\nabla h\| = \sqrt{\left(\frac{\partial h}{\partial x}\right)^2 + \left(\frac{\partial h}{\partial y}\right)^2}. \tag{19}$$

Then, we map the divergence of the normalised gradient

$$\operatorname{div}\left(\frac{\nabla h}{\|\nabla h\|}\right). \tag{20}$$

Using this map, we can isolate zones of maximum and minimum curvature of the contour lines that directly indicate the presence of valleys and crests, respectively (see Figs. 6-12c).
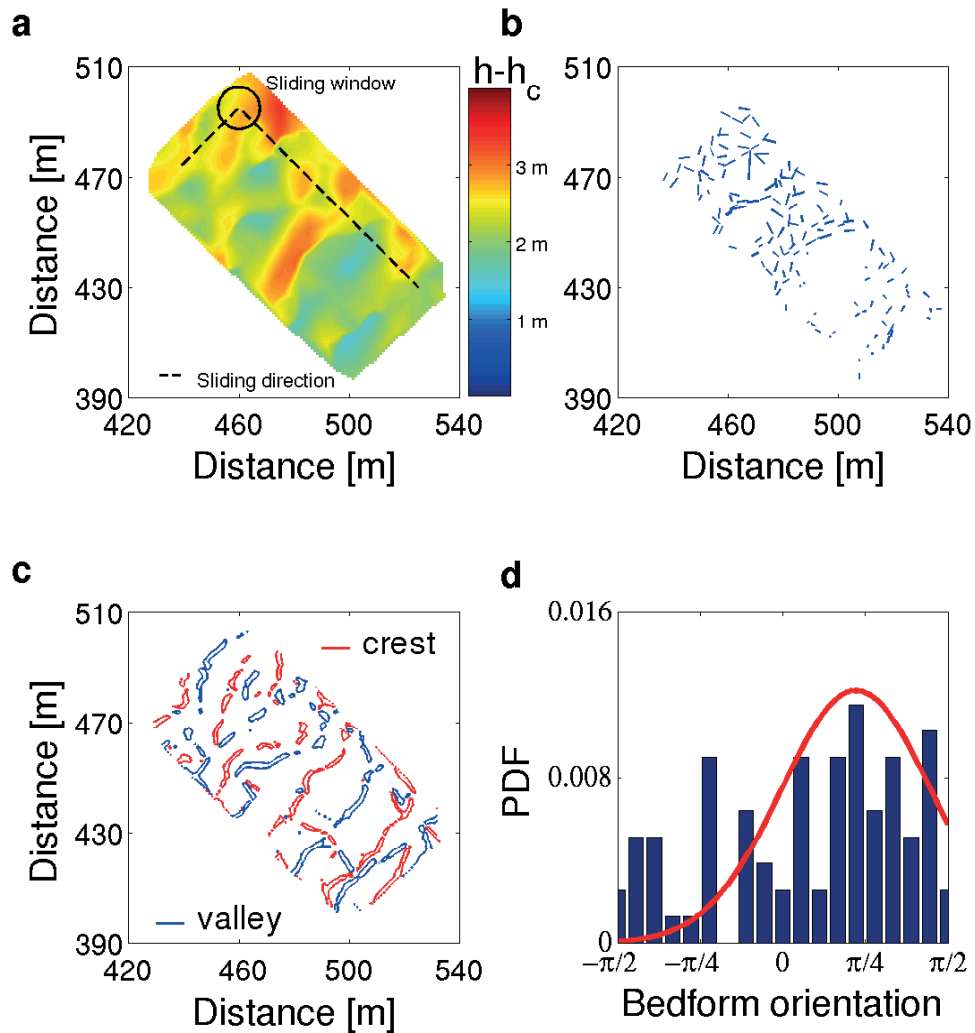
Figure 6: Orientation of bedforms on the 30$^{\text{th}}$ of April 2008. (a) Topography in the open corridor using a normalised colorbar. We analyse circular parcels of the open corridor using a sliding window (black circle) with a radius of 7.5 m and an offset of 10 m. The two sliding directions are northwest-southeast and southwest-northeast (dashed lines). h_c is the minimum elevation recorded in any survey. To concentrate on significant dune features, we take $h_t - h_c = 2$ m. (b) Principal direction of the topography associated with the largest eigenvalue of the mass distribution matrix. (c) Crests and valleys in the open corridor using the divergence of the normalised gradient. (d) Probability distribution function of the principal direction measured anticlockwise from East. A maximum in this distribution indicates a privileged bedform orientation. A fit by a normal distribution (red curve) gives a mean value of 40° (see Fig. 4a of the main manuscript).
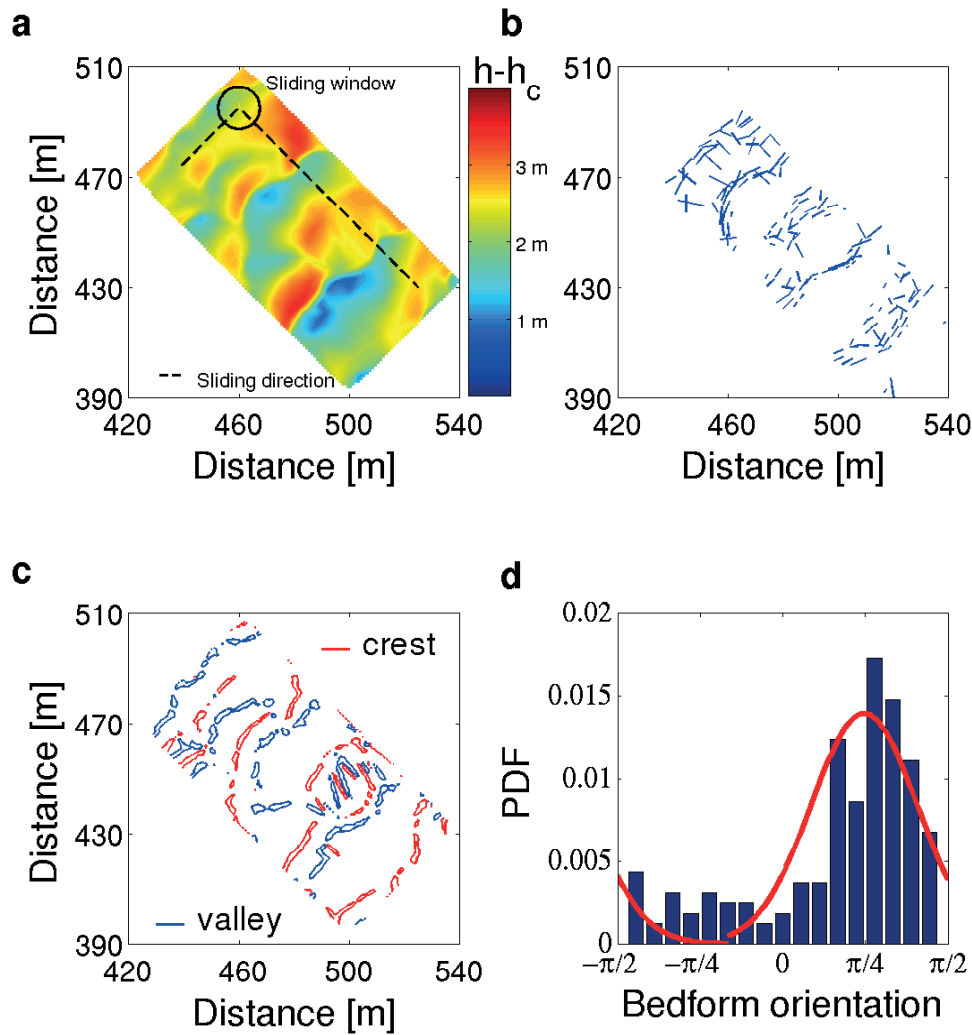
Figure 7: Orientation of bedforms on the 31st of March 2009. (a) Topography in the open corridor using a normalised colorbar. We analyse circular parcels of the open corridor using a sliding window (black circle) with a radius of 7.5 m and an offset of 10 m. The two sliding directions are northwest-southeast and southwest-northeast (dashed lines). h_c is the minimum elevation recorded in any survey. To concentrate on significant dune features, we take $h_t - h_c = 2$ m. (b) Principal direction of the topography associated with the largest eigenvalue of the mass distribution matrix. (c) Crests and valleys in the open corridor using the divergence of the normalised gradient. (d) Probability distribution function of the principal direction measured anticlockwise from East. A maximum in this distribution indicates a privileged bedform orientation. A fit by a normal distribution (red curve) gives a mean value of 44° (see Fig. 4a of the main manuscript).
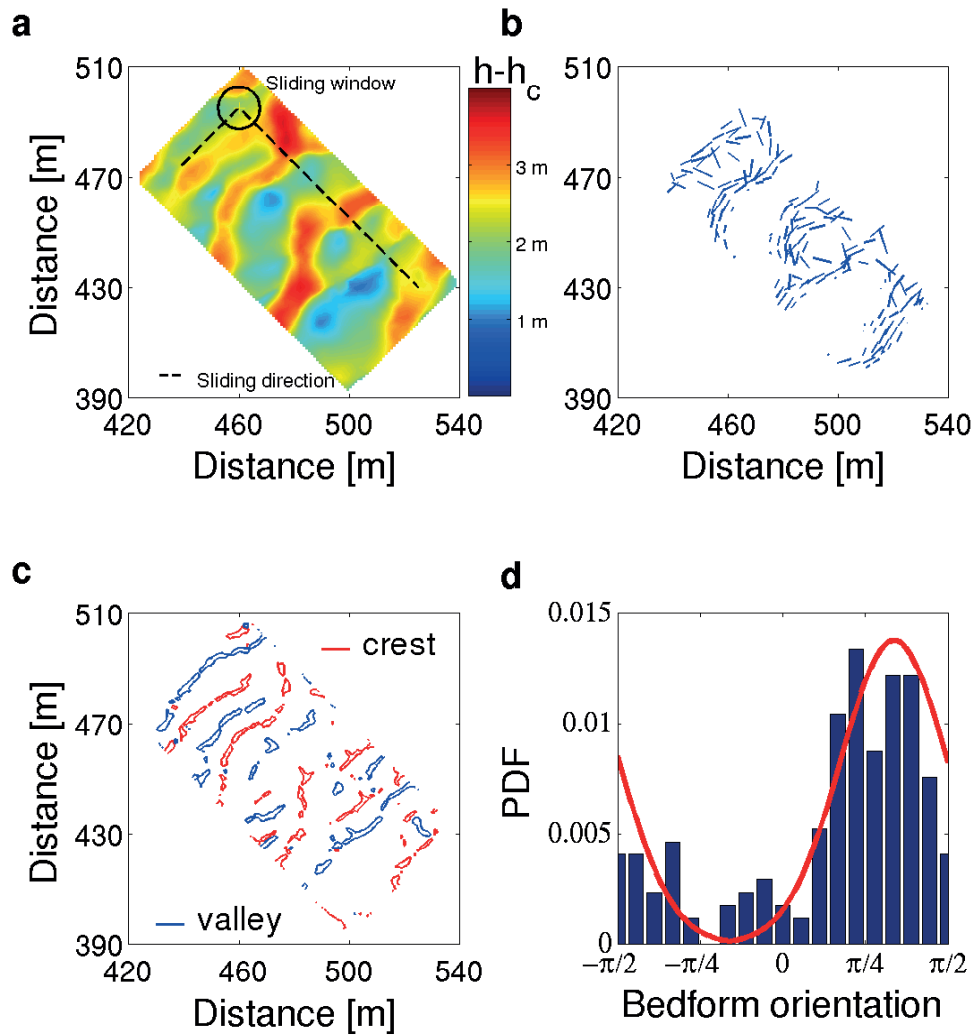
Figure 8: Orientation of bedforms on the 31st of October 2009. (a) Topography in the open corridor using a normalised colorbar. We analyse circular parcels of the open corridor using a sliding window (black circle) with a radius of 7.5 m and an offset of 10 m. The two sliding directions are northwest-southeast and southwest-northeast (dashed lines). h_c is the minimum elevation recorded in any survey. To concentrate on significant dune features, we take $h_t - h_c = 2$ m. (b) Principal direction of the topography associated with the largest eigenvalue of the mass distribution matrix. (c) Crests and valleys in the open corridor using the divergence of the normalised gradient. (d) Probability distribution function of the principal direction measured anticlockwise from East. A maximum in this distribution indicates a privileged bedform orientation. A fit by a normal distribution (red curve) gives a mean value of 61° (see Fig. 4a of the main manuscript).
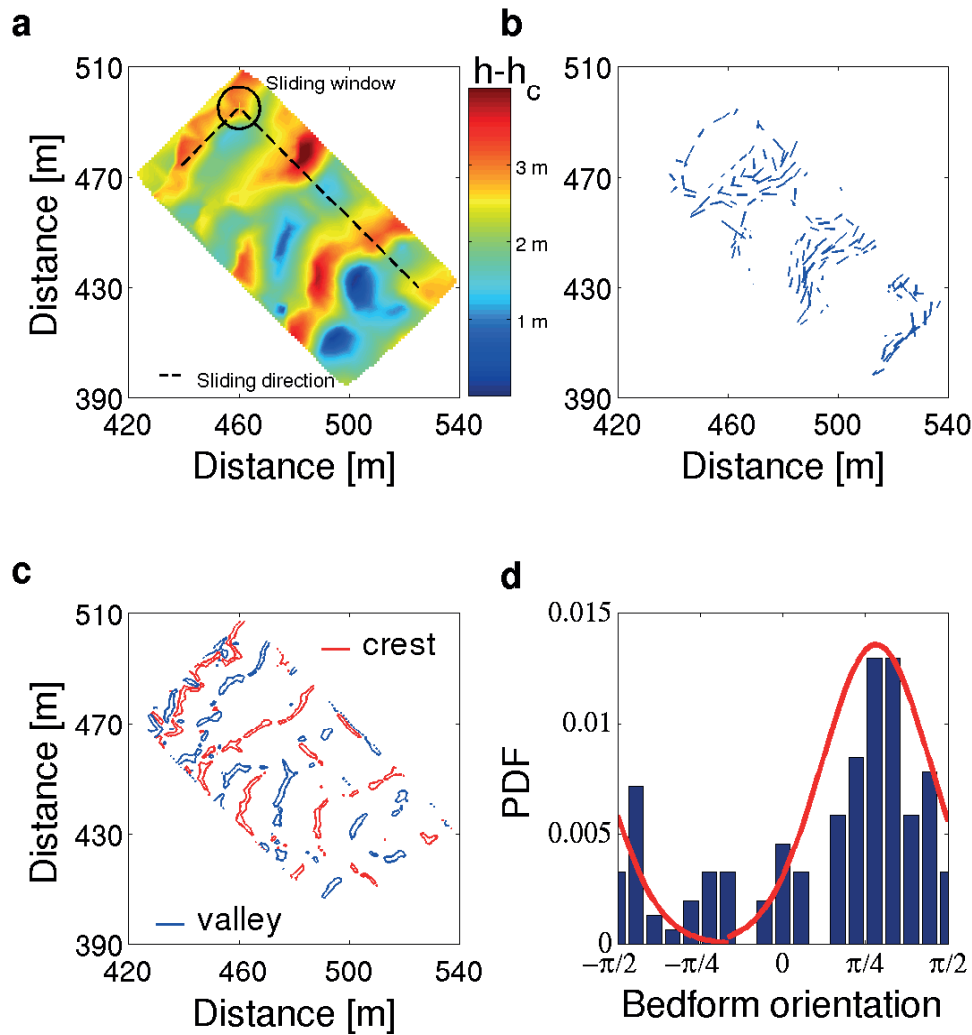
Figure 9: Orientation of bedforms on the 1st of June 2010. (a) Topography in the open corridor using a normalised colorbar. We analyse circular parcels of the open corridor using a sliding window (black circle) with a radius of 7.5 m and an offset of 10 m. The two sliding directions are northwest-southeast and southwest-northeast (dashed lines). h_c is the minimum elevation recorded in any survey. To concentrate on significant dune features, we take $h_t - h_c = 2$ m. (b) Principal direction of the topography associated with the largest eigenvalue of the mass distribution matrix. (c) Crests and valleys in the open corridor using the divergence of the normalised gradient. (d) Probability distribution function of the principal direction measured anticlockwise from East. A maximum in this distribution indicates a privileged bedform orientation. A fit by a normal distribution (red curve) gives a mean value of 51° (see Fig. 4a of the main manuscript).
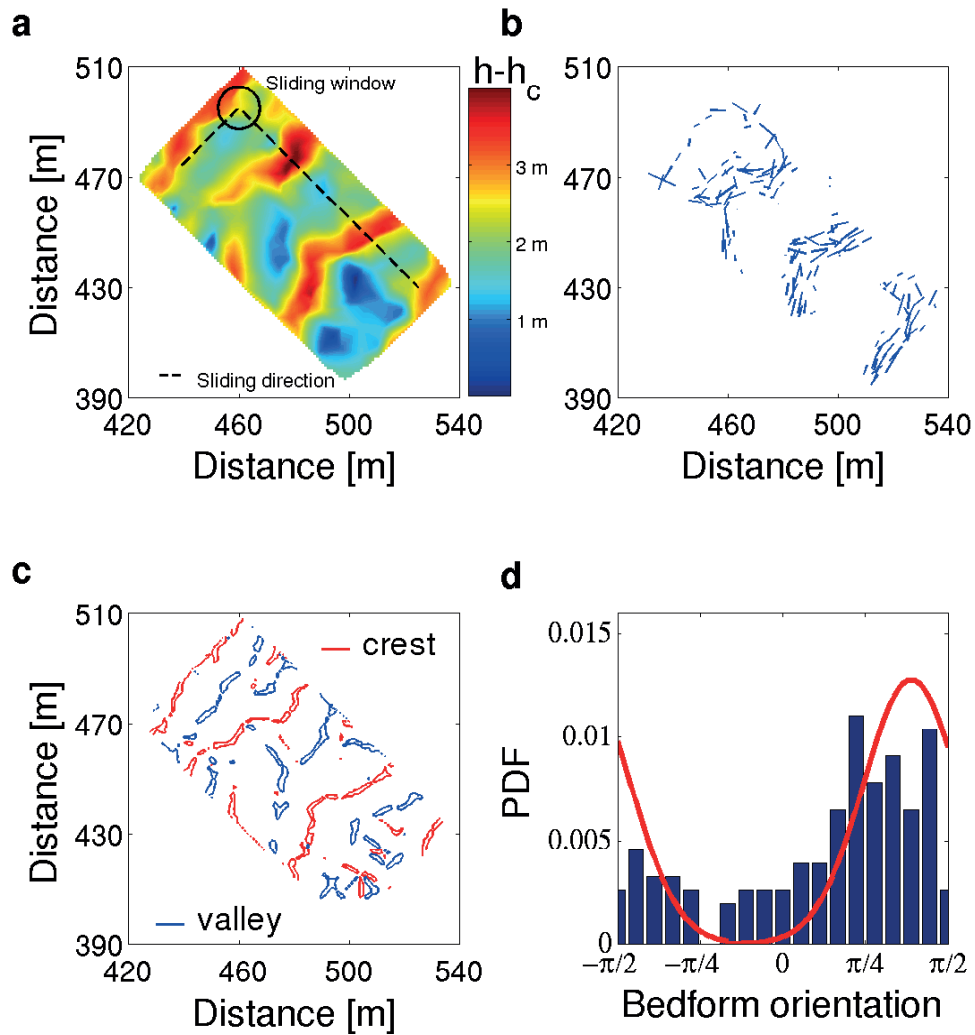
Figure 10: Orientation of bedforms on the 31st of October 2010. (a) Topography in the open corridor using a normalised colorbar. We analyse circular parcels of the open corridor using a sliding window (black circle) with a radius of 7.5 m and an offset of 10 m. The two sliding directions are northwest-southeast and southwest-northeast (dashed lines). h_c is the minimum elevation recorded in any survey. To concentrate on significant dune features, we take $h_t - h_c = 2$ m. (b) Principal direction of the topography associated with the largest eigenvalue of the mass distribution matrix. (c) Crests and valleys in the open corridor using the divergence of the normalised gradient. (d) Probability distribution function of the principal direction measured anticlockwise from East. A maximum in this distribution indicates a privileged bedform orientation. A fit by a normal distribution (red curve) gives a mean value of 74° (see Fig. 4a of the main manuscript).
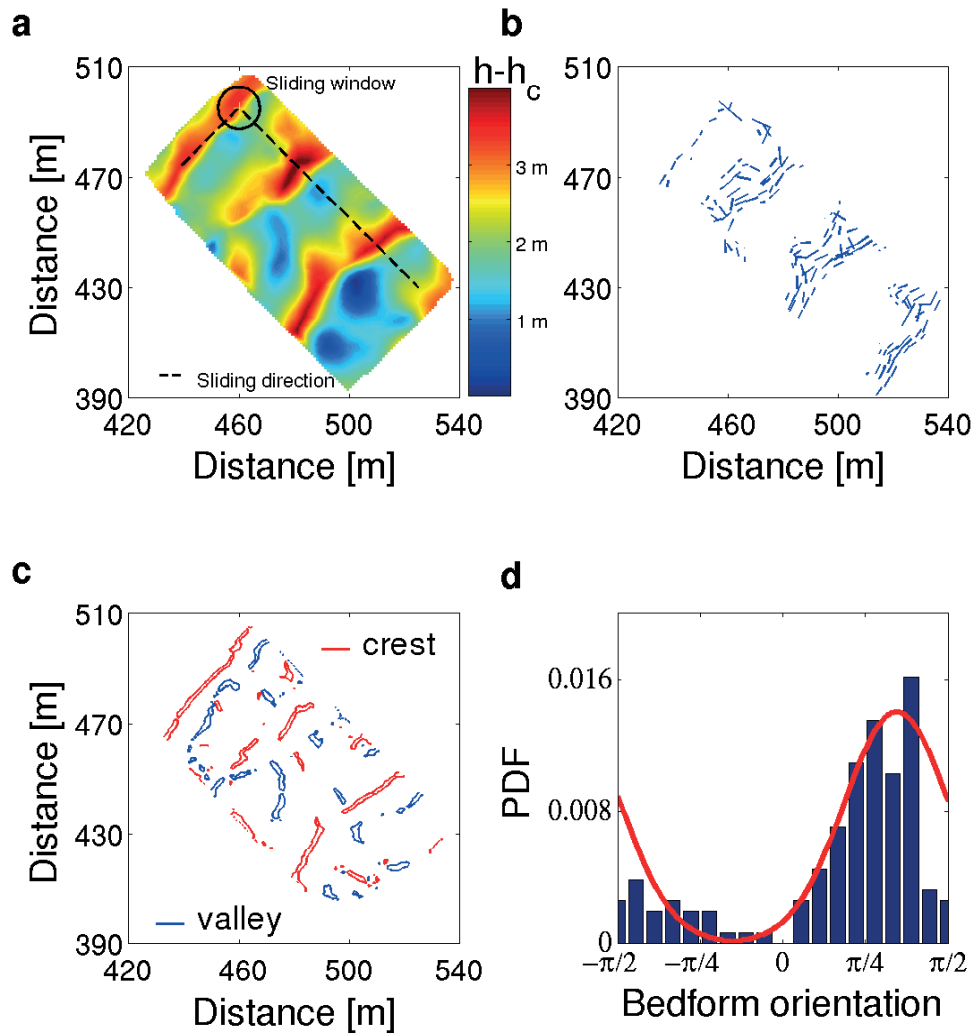
Figure 11: Orientation of bedforms on the 30th of April 2011. (a) Topography in the open corridor using a normalised colorbar. We analyse circular parcels of the open corridor using a sliding window (black circle) with a radius of 7.5 m and an offset of 10 m. The two sliding directions are northwest-southeast and southwest-northeast (dashed lines). h_c is the minimum elevation recorded in any survey. To concentrate on significant dune features, we take $h_t - h_c = 2$ m. (b) Principal direction of the topography associated with the largest eigenvalue of the mass distribution matrix. (c) Crests and valleys in the open corridor using the divergence of the normalised gradient. (d) Probability distribution function of the principal direction measured anticlockwise from East. A maximum in this distribution indicates a privileged bedform orientation. A fit by a normal distribution (red curve) gives a mean value of 63° (see Fig. 4a of the main manuscript).
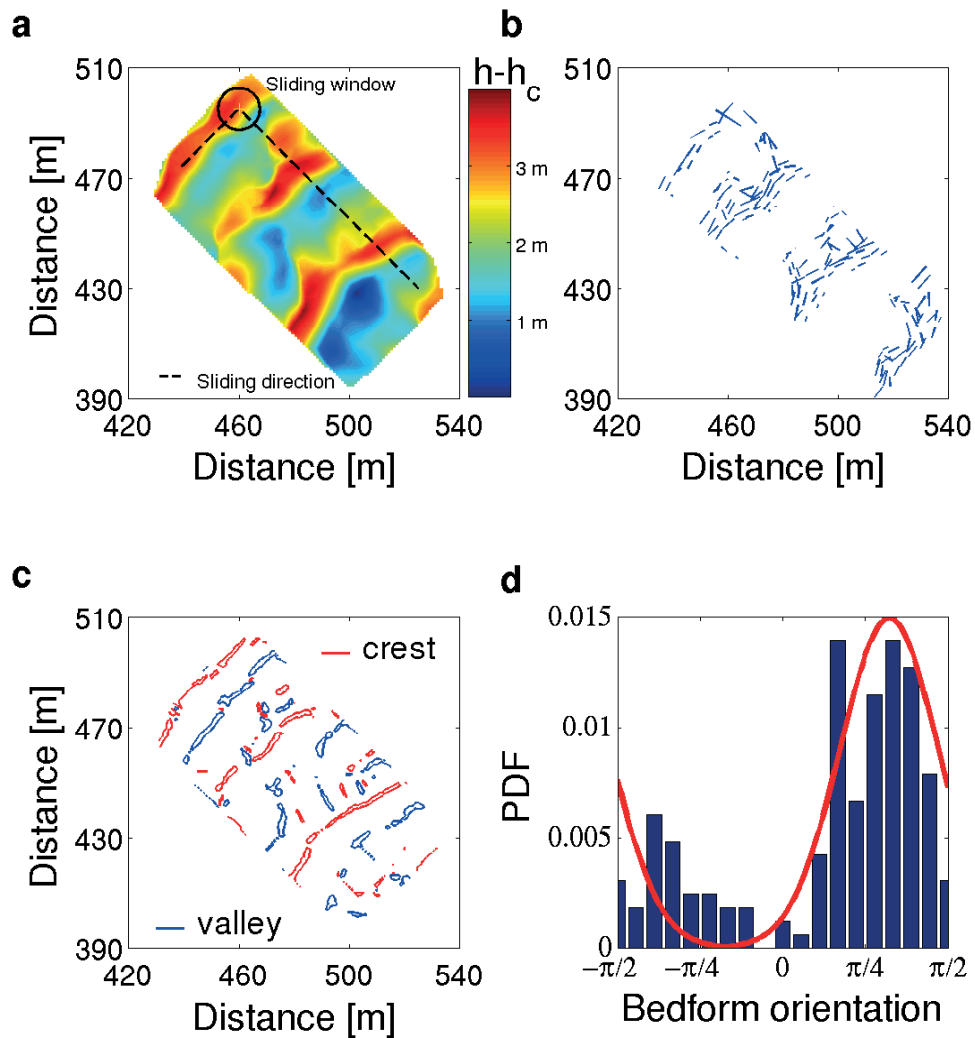
Figure 12: Orientation of bedforms on the 31st of October 2011. (a) Topography in the open corridor using a normalised colorbar. We analyse circular parcels of the open corridor using a sliding window (black circle) with a radius of 7.5 m and an offset of 10 m. The two sliding directions are northwest-southeast and southwest-northeast (dashed lines). h_c is the minimum elevation recorded in any survey. To concentrate on significant dune features, we take $h_t - h_c = 2$ m. (b) Principal direction of the topography associated with the largest eigenvalue of the mass distribution matrix. (c) Crests and valleys in the open corridor using the divergence of the normalised gradient. (d) Probability distribution function of the principal direction measured anticlockwise from East. A maximum in this distribution indicates a privileged bedform orientation. A fit by a normal distribution (red curve) gives a mean value of 58° (see Fig. 4a of the main manuscript).
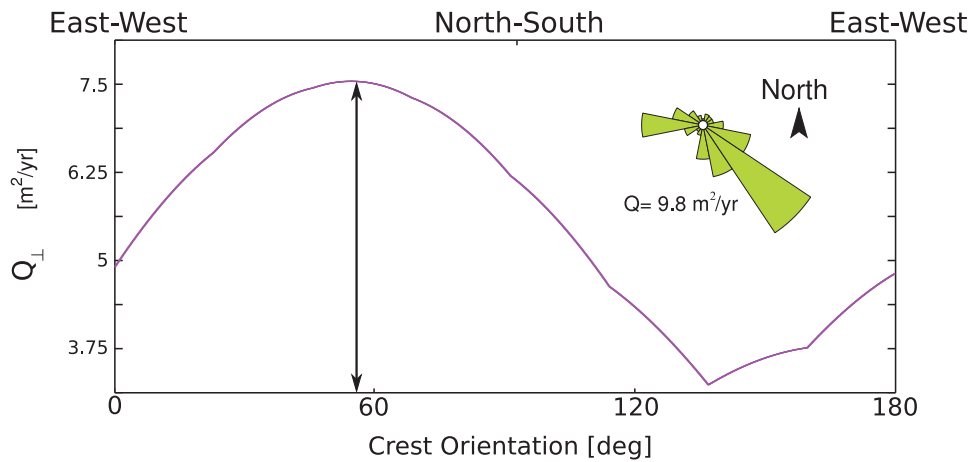
Figure 13: Estimation of crest orientation using the cross-crest components of transport. For all dune crest orientation $\alpha \in [0; \pi]$ measured anticlockwise from East, we calculate $Q_\perp$, the sum of the normal components of the transport vectors (see Eq. 21). The crest orientation predicted the gross bedform-normal transport rule corresponds to the maximum $Q_\perp$-value (black arrow). Here we have a predicted orientation of 58°. The inset shows the sand flux rose that we use to calculate the cross-crest components of transport. This fluxes are derived from the wind data from the 1st of January 2008 to the 31st of December 2011 (see Eq. 3).

4 Testing the gross bedform-normal transport rule on wind data

Rubin and Hunter [1987] propose that dune crests have the orientation for which the sum of the normal components of the transport vectors reaches its maximum. Mainly discussed for two asymmetric winds with a divergence angle larger than 90°, this gross bedform-normal transport rule can be generalised to all wind regimes. Following *Rubin and Ikeda* [1990], we use the wind data to estimate the sum of the cross-crest components of transport for all possible dune orientations $\alpha \in [0; \pi]$. Then, using the same notation as in Sec. 1.1 the gross normal transport writes

$$Q_\perp(\alpha) = \frac{\sum\limits_{i=2}^{N} \|\mathbf{Q}_{\text{sat}}^i\|(t_i - t_{i-1}) \, |\sin(\beta_i - \alpha)|}{\sum\limits_{i=2}^{N}(t_i - t_{i-1})}, \quad (21)$$

where β_i is the wind direction at time t_i.

Using this technique, Fig. 13 shows that the predicted crest orientation is approximately of 58° when measured anticlockwise from East. Fig. 4a on the main manuscript show the predictions for different time periods from

the flattening time. On the other hand, the resulting sand flux measured on a flat sand bed is oriented at -71°. Then, there is an angle of approximately 50° between the strike of crestline and the resultant sand flux. Hence, the emergent bedforms of the landscape-scale experiment are oblique dunes.

The wavelength and the amplitude of the surface undulations in the open corridor are calculated from the autocorrelation function of the bed profile $C(l,t) = \langle h(x,t)h(x+l,t)\rangle - \langle h(x,t)\rangle^2$ using 70 transects aligned with the northwest-southeast direction of the open corridor and separated by 1 meter. The amplitude is the mean value of $A(t) = 2\sqrt{2C(0,t)}$ (Fig. 2a of the main manuscript). The wavelength is the mean position of the first peak corrected for the final dune orientation (Fig. 2b of the main manuscript). Error bars are the corresponding standard deviations for all transects.

References

Iversen, J., and K. Rasmussen, The effect of wind speed and bed slope on sand transport, *Sedimentology*, *46*, 723–731, 1999.

Rubin, D., and R. Hunter, Bedform alignment in directionally varying flows, *Science*, *237*, 276–278, 1987.

Rubin, D., and H. Ikeda, Flume experiments on the alignment of transverse, oblique, and longitudinal dunes in directionally varying flows, *Sedimentology*, *37*, 673–684, 1990.

Ungar, J. E., and P. K. Haff, Steady state saltation in air, *Sedimentology*, *34*, 289–299, 1987.